Intrinsic defects in lymph node stromal cells underpin poor germinal center responses during aging

Alice E Denton[1,7,9]*, Alyssa Silva-Cayetano[1], James Dooley[1,2], Danika L Hill[1, 3], Edward J Carr[1,4], Philippe Robert[5,8], Michael Meyer-Hermann[5,6], Adrian Liston[1,2] and Michelle A Linterman[1]*

[1] Laboratory of Lymphocyte Signalling and Development, Babraham Institute, Cambridge CB22 3AT UK
[2] Adaptive Immunology Laboratory, VIB and University of Leuven, Leuven 3000 Belgium
[3] Department of Immunology and Pathology, Central Clinical School, Monash University and Alfred Hospital, Melbourne, Victoria 3004, Australia
[4] Department of Medicine, University of Cambridge, Cambridge CB2 0QQ UK
[5] Systems Immunology and Integrated Centre of Systems Biology, Helmholtz Centre for Infection Research, Braunschweig 38124 Germany
[6] Institute for Biochemistry, Biotechnology and Bioinformatics, Technische Universität Braunschweig, Braunschweig 38124 Germany and Cluster of Excellence RESIST (EXC 2155), Hannover Medical School, Hannover, Germany
[7] Current address: Department of Immunology and Inflammation, Imperial College London, London W12 0NN UK
[8] Current address: Department of Clinical Immunology, Oslo University, Oslo, Norway
[9] Lead contact
*Correspondence: a.denton@imperial.ac.uk or michelle.linterman@babraham.ac.uk

Highlights

- The stromal cell response to immunization is impaired in aged mice
- Immunization induces remodeling of marginal reticular cells
- Age impairs MRC activation and proliferation
- Heterochronic parabiosis identifies that age-associated defects in the microenvironment underpin poor GC responses

Summary

The failure to generate enduring humoral immunity after vaccination is a hallmark of advancing age. This can be attributed in part to a reduction in the germinal center response, which generates long-lived antibody-secreting cells that provide protection against (re)infection. Despite intensive investigation into the effect of age on the lymphoid compartment, how age impacts on the stromal cell compartment is not understood. Herein we demonstrate that ageing reduces the capacity of germinal center-associated stromal cells to respond to vaccination. Heterochronic parabiosis demonstrates that the age of the microenvironment dictates the size of the germinal center response, irrespective of the age of immune cells. This study reveals that age-associated defects in stromal cells are a significant barrier to efficacious vaccine responses in older individuals.

Keywords

Germinal center, lymph node stromal cells, follicular dendritic cell, ageing, marginal reticular cell, immunization, vaccination

Introduction

While the extension of human life expectancy is a great achievement of the modern era, it creates a challenge for science: to facilitate healthy ageing. Older individuals are at particular risk of infection, and this is in part caused by decreased functionality of the immune system (Montecino-Rodriguez et al., 2013). Vaccination is an effective preventative

strategy for limiting the negative health consequences from infection, however older persons often do not generate long-lasting protective immunity after vaccination (Ciabattini et al., 2018; Goodwin et al., 2006; Govaert et al., 1994; Weinberger and Grubeck-Loebenstein, 2012). Therefore, an understanding of why older individuals do not respond well to vaccines is key to developing the next generation of immunization strategies that are effective in older persons.

The generation of lasting protective immunity requires the generation of long-lived plasma cells that produce high affinity class-switched antibodies (Weisel et al., 2016). Plasma cells are the ultimate output of the germinal center (GC), a specialized immune response that forms in secondary lymphoid organs (Stebegg et al., 2018). The GC reaction requires the concerted efforts of many different cell types that must be coordinated in time and space: B cells, T follicular helper (Tfh) cells, dendritic cells and macrophages are brought together upon a network of specialized stromal cells that provide migratory cues that direct cells to, and within, the GC (Denton and Linterman, 2017).The GC is a polarized structure with two functionally distinct compartments known as light and dark zones (Allen et al., 2004; Bannard et al., 2013). In the dark zone, GC B cells proliferate and the genes encoding the B cell receptor undergo somatic hypermutation. Because of the random nature of somatic hypermutation, selection must occur to ensure this process has not negatively impacted on the function or specificity of the B cell receptor and increases receptor affinity. To do this, GC B cells move to the light zone where they can receive help from a specialized subset of $CD4^+$ T cells, Tfh cells (Vinuesa et al., 2016). GC B cells that received help from Tfh cells then migrate back to the dark zone and either undergo further rounds of proliferation and mutation or differentiate into memory B cells or long-lived antibody-secreting cells that exit the GC (Stebegg et al., 2018).

Stromal cells are critical to lymph node structure, dictating the T and B cell areas and directly regulating immune cell homeostasis and adaptive immune responses (Cremasco et al., 2014; Denton et al., 2014; Krishnamurty and Turley, 2020). Stromal cells form the physical scaffold upon which immune cells migrate and produce molecules that dictate the migration and survival of immune cells (Alexandre and Mueller, 2018; Bajenoff et al., 2006; Link et al., 2007). There is significant diversity in the types of lymph node stromal cells (Rodda et al., 2018); for the GC, two key stromal cells are known to dictate its structure and function. The light zone is supported by follicular dendritic cells (FDCs), which are essential for the GC (Wang et al., 2011) as they produce CXCL13 and act as a depot for antigen (Allen and Cyster, 2008). The dark zone is populated by CXCL12-abundant reticular cells whose functions are poorly defined outside of their role as a migratory nexus (Bannard et al., 2013; Rodda et al., 2015). A third cell type, marginal reticular cells (MRCs), may also play important roles in GC formation as they may contribute to antigen transport (Katakai, 2012; Katakai et al., 2008) and can act as a progenitor for *de novo* FDC differentiation (Jarjour et al., 2014).

A reduction in the size, quality and output of the GC in older individuals is observed in a number of infection and vaccination settings (Boraschi et al., 2013; Goronzy and Weyand, 2013; Kosco et al., 1989; Szakal et al., 1990). This has been linked to T cell-intrinsic mechanisms (Eaton et al., 2004; Garcia and Miller, 2001; Sage et al., 2015; Yang et al., 1996), and changes in the microenvironment (Becklund et al., 2016; Lefebvre et al., 2012; Richner et al., 2015; Stebegg et al., 2020; Turner and Mabbott, 2017a). Age reduced the ability of FDCs to capture and retain antigen (Aydar et al., 2002, 2003; Szakal et al., 1990), suggesting an impaired functionality in ageing that may underpin poor GC formation. However, apart from changes in antigen capture by FDC, we do not know how GC stromal cells are influenced by age and what contribution any cell-intrinsic changes make to the defective GC

reaction. We show here that aged FDCs and MRCs respond poorly to immunization, at a cellular and molecular level. MRCs are particularly affected, with age causing a reduction in their proliferative response to immunization that limits the expansion of the FDC network through *de novo* differentiation. We use heterochronic parabiosis to demonstrate that the poor responsiveness of stromal cells directly impairs the capacity of B cells to participate in a GC, independent of B cell age. In sum, this study describes the impact of age on the transcriptional and cellular responses of MRCs and FDCs to immunization and emphasizes that these defects in stromal cell responses may underpin the poor GC response in aged individuals.

Results

Ageing impairs stromal cell expansion in response to immunization

In order to understand how stromal cells are affected by ageing, and how these changes impact on the generation of GC responses to immunization, we subcutaneously immunized adult (8-12 week old) and aged (>95 week old) Balb/c mice. The ki67$^+$Bcl6$^+$B220$^+$ GC B cell response (Fig 1A) was reduced in both proportion (Fig 1B) and absolute number (Fig 1C) consistent with previous studies (Kosco et al., 1989; Stebegg et al., 2020; Szakal et al., 1990). To determine whether stromal cells were also affected by age, we analyzed the expansion of MRCs and FDCs, two stromal cell types typically associated with the GC (Denton and Linterman, 2017). MRCs and FDCs were defined as MAdCAM-1$^+$CD21/35$^-$ or MAdCAM-1$^+$CD21/35$^+$, respectively, amongst CD45$^-$CD31$^-$Pdpn$^+$ stromal cells (Fig 1D). We observed a trend towards a reduction in MRCs as a proportion of CD45$^-$CD31$^-$Pdpn$^+$ stromal cells seven days after immunization (Fig 1E) and a 6-fold reduction in the absolute number of MRCs at the same timepoint (Fig 1F). This early defect in MRC number was associated with a reduction in the proportion and number of FDCs in aged mice (Fig 1G, H), compared to adult Balb/c mice. To determine whether these results were consistent between strains of mice, we immunized C57BL/6 mice and determined the GC B cell (Fig 1I-K) and stromal cell (Fig 1L-P) responses seven days after immunization. We found that both the proportion (Fig 1I, J) and absolute number (Fig 1K) of GC B cells was reduced in aged mice. Likewise, we saw a significant reduction in both the proportion and absolute number of MRCs (Fig 1L-N) and FDCs (Fig 1L, O, P) in aged mice seven days after immunization. Taken together, these data show that age impairs the expansion of stromal cells that are associated with the GC.

The size of the FDC network is a key contributor to GC output

The age-dependent changes in FDC responses to immunization was confirmed in stained cryosections of lymph nodes obtained 14 days after immunization of adult (8-12 week old) and aged (90-95 week old) Balb/c mice (Fig 2A). Both the FDC area (Fig 2B), as a measured by the cross-sectional area of the CD35$^+$ region within IgD$^-$ GCs, and the proportion of the GC that was occupied by FDCs (Fig 2C) was significantly reduced (1.7-fold) in the lymph nodes from aged mice.

In the absence of an *in vivo* tool to specifically reduce the FDC network we used the *hyphasma* mathematical modelling approach (Meyer-Hermann et al., 2012; Meyer-Hermann and Maini, 2005) to understand whether a reduced FDC network would be predicted to alter GC size or output. To model the age-associated changes in the size of the FDC network, we reduced the size of the FDC network by decreasing both the proportion of the GC that was covered by FDCs (control 50%, test 30%) and the number of FDCs (control 200 cells, test 100 cells). We did not alter the total level of antigen on the surface of FDCs, allowing us to determine the effect of FDC network size independent of antigen capture. These changes maintain the same FDC density, resulting in FDCs being positioned closer to the light zone (Fig 2D), thus mimicking the reduction in GC light zone (Fig 2A-C) and the reduction in the

number of FDCs (Fig 1) observed in aged mice. Reducing the FDC network has a significant impact on the GC: the number of GC B cells at day seven (Fig 2E) and the number of GC output cells at day 21 (Fig 2F) are reduced when the FDC network resembles the aged state. This phenocopies our experimental data from aged mice (Fig 1), suggesting that poor expansion of the FDC network contributes to the impaired GC response in aged mice independently of antigen captured and retention.

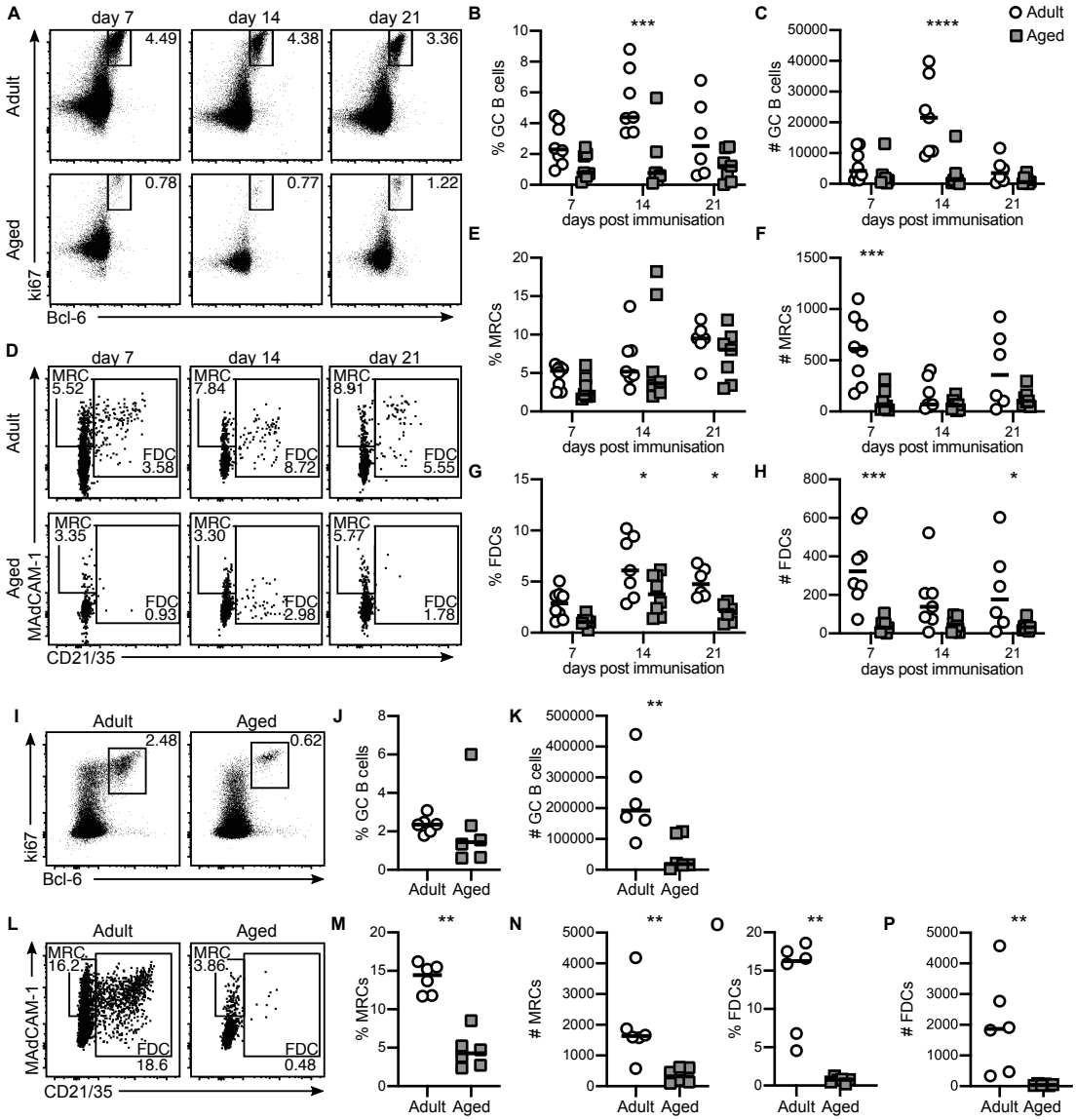

Figure 1. Ageing diminishes the GC and stromal cell response to immunization. Adult (8-12 week old) and aged (>98 week old) mice were immunized subcutaneously with 50µg NP-KLH emulsified in Alum and the stromal and immune cell responses were determined. (A-H) GC B cell and stromal cell responses were determined in Balb/c mice seven, 14 and 21 days after immunization. (A) Representative gating of Bcl-6$^+$ki67$^+$ GC B cells. (B-C) The proportion (B) and absolute number (C) of GC B cells at different times after immunization. (D-H) stromal cell responses were determined for the same timepoints as in (A-C). (A) Representative gating of MRCs (MAdCAM-1$^+$CD21/35$^-$) and FDCs (CD21/35$^+$) amongst CD31$^-$CD45$^-$Pdpn$^+$ stromal cells. (E-H) The proportion (E, G) and absolute number (F, H) of MRCs (E, F) and FDCs (G, H). (I-P) GC B cell and stromal cell responses were determined in C57BL/6 mice seven after immunization. (I-J) GC B cells were gated as Bcl-6$^+$ki67$^+$ (I), and the proportion (J) and absolute number (K) of GC B cells was determined. (L-P) MRCs and FDCs were gated based on CD21/35 and MAdCAM-1 staining amongst CD31$^-$CD45$^-$Pdpn$^+$ stromal cells (L) and the proportion (M, O) and absolute number (N, P) or MRCS (M, N) and FDCs (O, P) was determined. Each symbol represents a biological replicate and lines indicate the median. Data are representative of at least two independent experiments with 6-8 mice per group. Statistical significance was determined using a Mann-Whitney rank test. * $p<0.05$, ** $p<0.01$ *** $p<0.001$ **** $p<0.0001$.

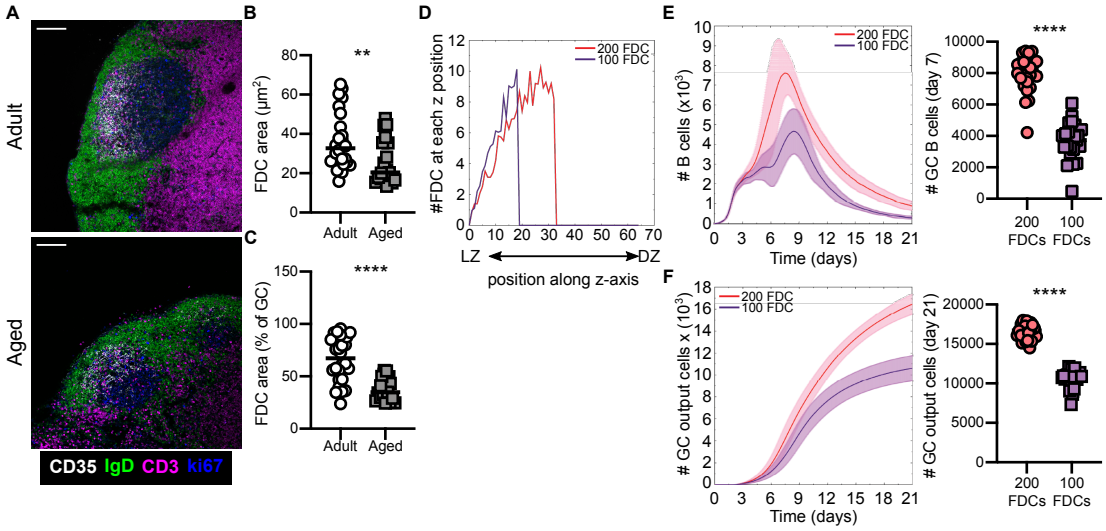

Figure 2. Mathematical modelling of the FDC network size impacts on GC output. (A-C) Cryosections from lymph nodes obtained 14 days after immunization of 12 week old (adult) or >90 week old (aged) Balb/c mice and stained for CD35 (white), IgD (green), CD3 (magenta) and ki67 (blue). Shown are representative images (A) and calculations of the cross-sectional area of the FDC network (B) and the proportion of the GC that is occupied by FDCs (C). Each dot represents a single GC, with data compiled from five individual mice per group. Statistical significance was conducted using a Mann-Whitney rank test. * p<0.05, **p<0.01 ***p<0.001 ****p<0.0001. Scale bars 100µm. (D-F) Mathematical modelling of the impact of reduced FDC area on the generation of GC B cells using *hyphasma*. (D) Spatial representation of the number of FDCs and positioning along the z-axis. (E) Total number of B cells generated through the GC reaction. Left: model output, right: graphical representation of number of GC B cells at day seven. (F) Total number of output GC B cells. Left: model output, right: graphical representation of number of output GC B cells at day 21. Lines in kinetic plots represent the mean of 25 simulations and shaded areas indicate the standard deviation. For graphs, each dot represents a simulation and lines indicate the median. Statistical significance was conducted using a Kruskal-Wallis test with Dunn's multiple testing correction. ****p<0.0001.

Aging impairs the stromal cell transcriptional response to immunization

Having established that the number of FDCs in a mature GC is reduced in age, and that mathematical modeling implicated this defect in reduced GC responses, we wanted to understand if there were transcriptomic differences in how FDCs respond to immunization, and how this is altered with advancing age. To address these questions, we performed RNA sequencing on sort-purified FDCs (CD21/35^{+}MAdCAM-1^{+}Pdpn-CD31^{-}CD45^{-}) isolated from lymph nodes of adult and aged mice both prior to and two days after immunization. We elected to study FDCs isolated from early after immunization in order to understand how the immunization directly affects the transcriptome of FDCs, rather than capturing changes that are secondary to the initiation of adaptive immune responses and minimizing the risk of confounding due to the differences in FDC number. FDC identity was confirmed by the lack of immune and endothelial cell-related gene expression (Fig S1A) and high expression of known FDC-associated genes (Rodda et al., 2018), including *Cxcl13*, *Cxcl12*, *Cr2*, *Fcgr2b* and *Pthlh* (Fig S1B, C); the reduction in *Fcgr2b* in aged FDCs is consistent with previous studies (Aydar et al., 2003). Principal component analysis (PCA) of all expressed genes revealed that there was little structure to the data that could be explained by age or immunization (Fig 3A). Supervised analysis of the transcriptome of FDCs revealed minor gene expression changes driven by age or immunization. In resting FDCs, age significantly affected the expression of 105 genes, with 38 genes more highly expressed in adult FDCs and 67 genes more highly expressed in aged FDCs (Fig 3B, Fig S2A, B). Immunization significantly affected the expression of 110 genes in adult FDCs, with 57 genes more highly expressed in responding FDCs and 53 genes more highly expressed in naive FDCs (Fig 3C, Fig S2D, E). Immunization of aged mice induced far fewer changes in FDCs than observed in adult mice, where only 44 genes were differentially expressed, of which 21 were more highly expressed

after immunization and 23 more highly expressed in unimmunized FDCs (Fig 3D, Fig S1E, F). Very little overlap was observed in the immunization-induced gene expression changes between adult and aged FDCs (Fig 3E), suggesting that the global transcriptional response to immunization in FDCs, whilst modest, was deregulated in the aged setting. The lack of a clear transcriptional signature suggests that early impaired responsiveness of FDCs to immunization may not be central to the defect in stromal cells observed in aged mice.

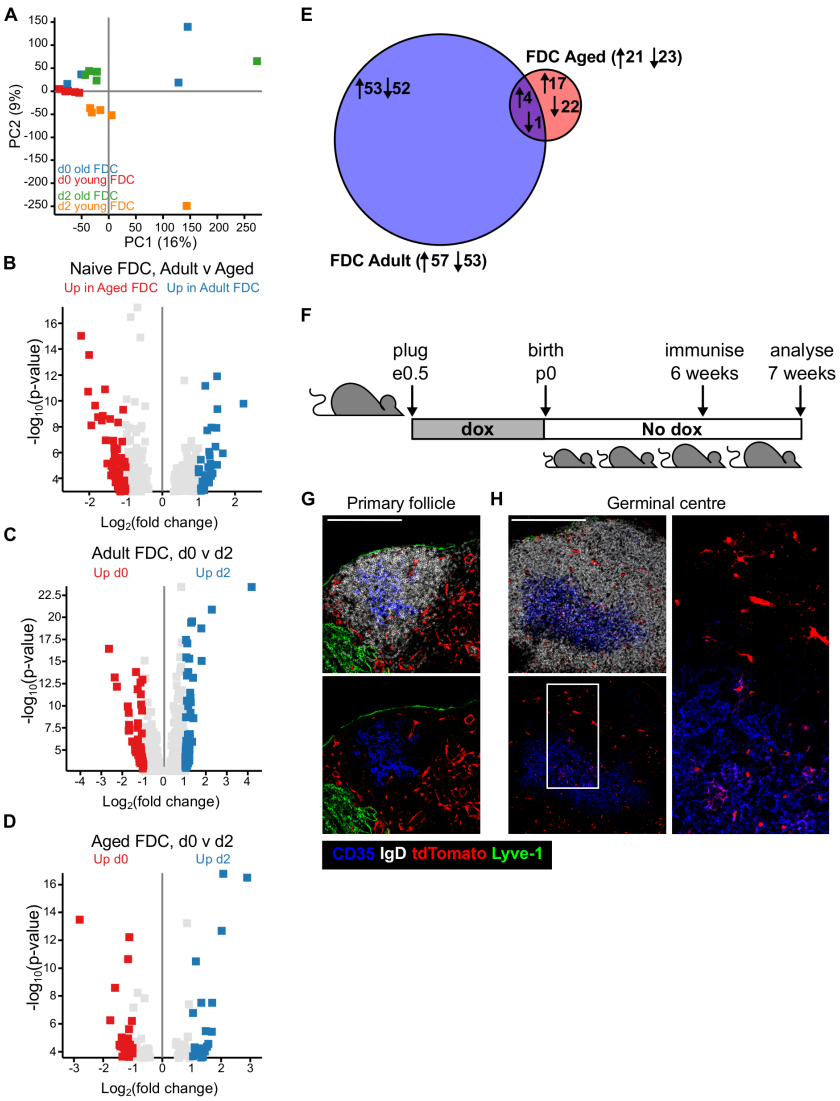

Figure 3. Transcriptional profiling of the FDC response to immunization in ageing. FDCs (CD21/35^{+}MAdCAM-1$^{+/-}$ Pdpn^{+}CD31^{-}CD45^{-}) were isolated from adult (8-12 week old) and aged (>98 week old) unimmunized mice, or mice immunized two days prior with 50µg NP-KLH emulsified in Alum, and their transcriptomes sequenced. (A) PCA of all expressed genes in all FDC samples. (B) Volcano plots showing all genes that are differentially expressed (DESeq2) between adult and aged FDCs isolated from unimmunized mice. Genes that are enriched in aged (red) or adult (blue) samples are highlighted. (C, D) Volcano plots showing all genes that are differentially expressed (DESeq2) between naïve and immunized FDCs in adult (C) and aged (D) mice. Genes that are enriched in unimmunized (blue) or immunized (red) are highlighted. (E) Comparison of differential gene expression following immunization in FDCs isolated from adult or aged mice, where the overlap shows genes that change in both adult and aged FDCs. (F-H) *FAP*^{tTA}::*TetO*^{Cre}::*R26R*^{tdTomato} mice were administered doxycycline from prior to conception until birth then maintained in the absence of doxycycline. At 6 weeks of age, mice were immunized and tissues taken for analysis seven days later (F). Cryosections (20µm) were prepared and stained for IgD (white), Lyve-1 (green) and CD35 (blue), alongside tdTomato (red). (G) lack of tdTomato labelling of FDCs in a primary B cell follicle in the non-draining lymph node. (H) tdTomato labelling of FDCs in a GC in the draining lymph node. Scale bars 200µm. Data in (A-F) are from five biological replicates except for the aged unimmunized FDC group, where four replicates were sequenced. Data in (J-K) are representative for four separate immunizations.

It has previously been suggested that MRCs can act as a precursor for *de novo* FDC differentiation in response to immunization in lymph nodes (Jarjour et al., 2014). To confirm this finding, we used a different lineage-tracing model, which is based on temporal control of fibroblast activation protein-alpha (FAP) expression (Denton et al., 2019). FAP-driven

labelling of stromal cells was inhibited during embryogenesis by administering doxycycline from conception until birth (e0-p0). At six weeks of age mice were immunized and the labelling of FDCs in GCs was assessed 7d later (Fig 3F). In this system, most T cell zone stromal cells and a small proportion of MRCs in primary B cell follicles are indelibly labelled with tdTomato (Fig 3G)(Denton et al., 2019). In GCs, which we defined by lack of IgD within an IgD^+ follicle, $tdTomato^+$ FDCs (Fig 3H) were observed, suggesting *de novo* FDC differentiation from non-FDCs, as FDCs do not express FAP (Denton et al., 2019; Denton et al., 2014). Because $tdTomato^+$ FDCs were linked in a chain to the follicle edge (Fig 3H, inset), we conclude that, as previously described (Jarjour et al., 2014), MRCs in the adult follicle can differentiate into FDCs following immunization.

These findings led us to hypothesize that ageing negatively impacts the capacity of MRCs to become FDCs, ultimately leading to impaired stromal cell expansion that is associated with poor GC formation. In order to test this, we performed bulk RNA sequencing of sort-purified MRCs, isolated from adult and aged lymph nodes both before and after immunization, based on MAdCAM-1 expression and a lack of CD21/35 expression amongst $Pdpn^+CD31^-CD45^-$ stromal cells. MRC identity was confirmed by the expression of markers typically associated with this cell type (Rodda et al., 2018), and lack of immune and endothelial cell-related markers (Fig S1A). MRCs expressed high levels of *Pdpn*, *Madcam1*, *Ccl19* and *Il7* compared to FDCs (Fig S1D), strongly suggesting an MRC phenotype, although their expression of *Tnfsf11* was relatively low. Adult MRCs obtained after immunization clustered distinctly from the other three groups by the first principle component (Fig 4A), suggesting that the transcriptome of adult responding MRCs is distinct from the other groups. Interestingly, when PC1 was plotted against PC3 we could observe separation of the different MRC groups (Fig 4B), suggesting that both age and immunization affected the transcriptome of MRCs. In the resting state, 122 genes were differentially expressed between aged and adult MRCs, with 25 genes more highly expressed in adult MRCs and 97 genes more highly expressed in aged MRCs (Fig 4C, Fig S3A, B). In response to immunization, the expression of 923 genes are significantly altered in adult MRCs: 378 are upregulated and 545 genes are downregulated after immunization (Fig 4D, Fig S3C, D). In comparison, just 101 genes are differentially expressed in aged MRCs (Fig 4E, Fig S3E, F). As observed for FDCs, very little overlap was observed between adult and aged MRCs in the genes that altered expression upon immunization (Fig 4F). In order to understand this further, we generated a list of genes that were differentially expressed upon immunization in adult MRCs but were not altered after immunization in aged MRCs and performed gene ontology analysis (Fig 4G, H). Amongst gene ontology terms that downregulated upon immunization, we saw a striking enrichment of genes associated with extracellular matrix synthesis and organization (Fig 4H, cyan), suggesting that MRCs may alter the local ECM to aid tissue remodeling, as has been described for fibroblastic reticular cells (Martinez et al., 2019). A number of gene ontology terms were significantly enriched in adult, but not aged, MRCs following immunization (Fig 4G). These can largely be classed as 'immune response' (magenta) or 'initiation of proliferation' (yellow), suggesting that in the aged setting MRCs are not adequately stimulated and fail to initiate a proliferative response. These data indicate that in younger adult mice, MRCs remodel their transcriptome early after immunization, but that this does not occur in aged mice, suggesting that MRCs fail to respond to vaccines in aged animals.

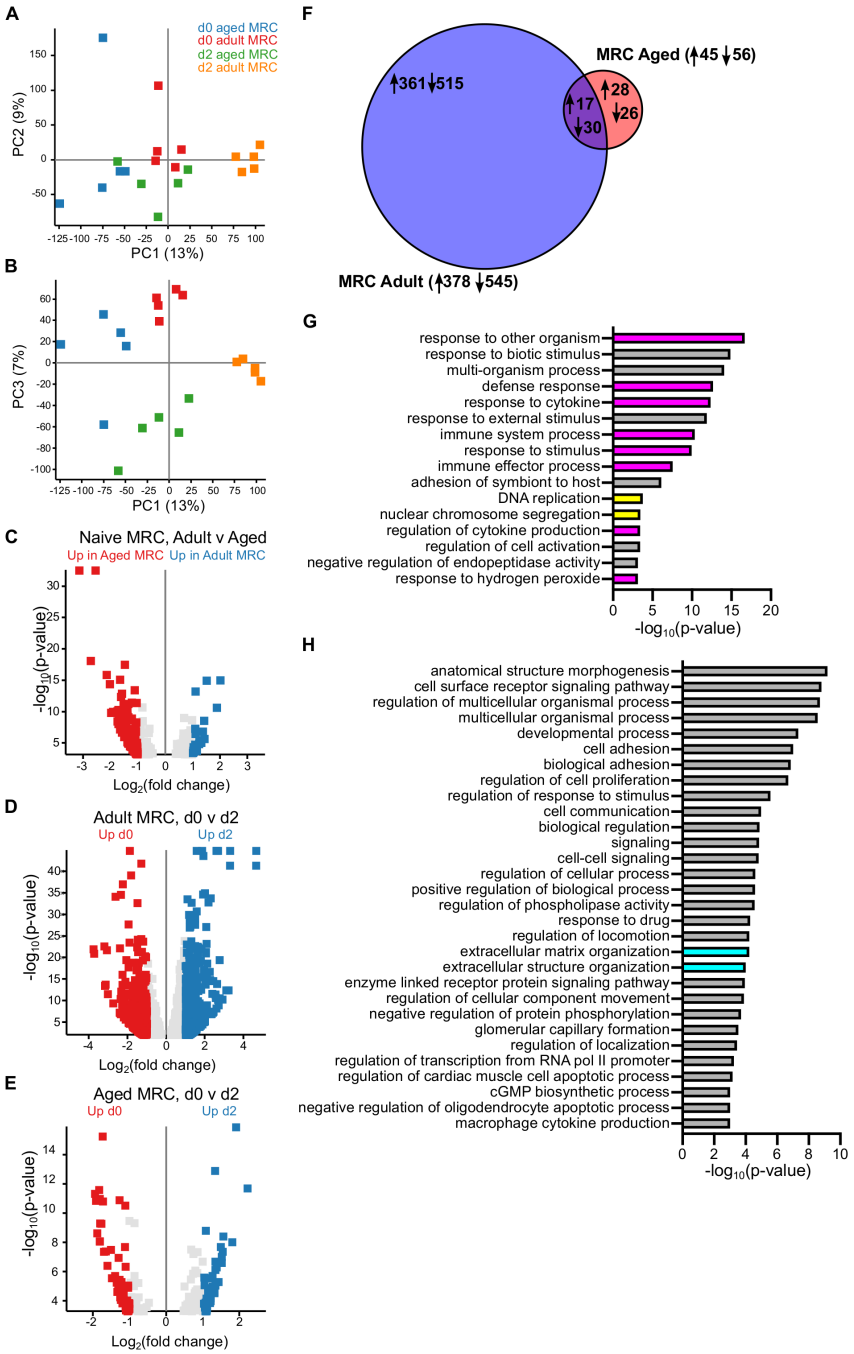

Figure 4. Transcriptional profiling of the MRC response to immunization in ageing. MRCs (CD21/35$^-$MAdCAM-1$^+$Pdpn$^+$CD31$^-$CD45$^-$) were isolated from adult (8-12 week old) and aged (>98 week old) unimmunized mice, or mice immunized two days prior with 50µg NP-KLH emulsified in Alum and subjected to RNA sequencing. (A-B) PCA of all expressed genes, showing PC1 v PC2 (A) and PC1 v PC3 (B). (C) Volcano plots of all genes that are differentially expressed (DESeq2) between adult and aged MRCs isolated from unimmunized mice. Genes that are enriched in aged (red) or adult (blue) are highlighted. (D, E) Volcano plots of all genes that are differentially expressed between naïve and immunized MRCs in adult (D) and aged (E) mice. Genes that are significantly enriched in unimmunized (blue) or immunized (red) are highlighted. (F) Comparison of differential gene expression following immunization in MRCs isolated from adult or aged mice, where the overlap shows genes that change in both adult and aged MRCs. Numbers indicate genes that are up/down regulated. (G, H) Gene set enrichment analysis was conducted using GOrilla and Revigo to identify gene sets that are uniquely enriched in adult MRCs after immunization. Shown are gene sets that are increased (G) or decreased (H) between d0 and d2 in adult MRCs at d2 but not changed between d0 and d2 in aged MRCs. Five biological replicates were sequenced for each group.

Failure to initiate MRC proliferation underpins the poor GC response to immunization

To investigate whether ageing negatively impacted on the capacity of MRCs to proliferate in response to immunization, we first determined the timecourse of the MRC proliferation after immunization. We found that MRC proliferation peaked four days after immunization (Fig 5A), in line with that previously described for MRCs (Jarjour et al., 2014). We then determined whether MRCs in aged mice could proliferate four days after immunization, based on the peak of the response in adult mice. We found that, as indicated by our sequencing results (Fig 4), a lower proportion of MRCs in aged mice expressed ki67 (Fig 5B,

C) indicating fewer proliferating cells. The proportion of FDCs expressing ki67 also peaked four days after immunization (Fig 5D). Aged mice had a trend for reduced proliferation, but this was not significant and was highly variable (Fig 5E, F). When we determined the expansion of MRCs four days after immunization, we found they were reduced by proportion (Fig 5G, H) and absolute number (Fig 5I) in aged mice. FDCs were also reduced in proportion (Fig 5G, J) and absolute number (Fig 5K) in aged mice; this reduction was so pronounced that FDCs were often not isolated from aged lymph nodes at this timepoint, potentially explaining the high variability in ki67 staining in aged FDCs (Fig 5F). We observed a reduction in the activation of MRCs (Fig 5L, M), as measured by the mean fluorescence intensity (MFI) of surface Pdpn staining (Yang et al., 2014), suggesting these cells were not as efficiently activated in an aged setting. The level of Pdpn expressed by FDCs four days after immunization was not affected by age (Fig 5N, O), perhaps indicative of an activation threshold for FDC differentiation. Because FDCs can be derived from MRCs (Jarjour et al., 2014), we next sought to determine whether aged MRCs have the capacity to differentiate into FDCs in general or whether this was a defect specific to vaccination.

Because FDC development in lymph nodes requires lymphotoxin-beta receptor signaling from B cells (Fu et al., 1998), B cell-deficient $uMT^{-/-}$ mice lack FDCs in adult lymph nodes. Adoptive transfer of B cells leads to FDC differentiation, and this is independent of MRC proliferation (Jarjour et al., 2014). We used the same model to understand MRC to FDC differentiation in ageing by adoptively transferring B cells purified from wildtype (6-8 week old) mice into adult (7 week old) or aged (>95 week old) $\mu MT^{-/-}$ mice. There was no difference in the engraftment of B cells between adult and aged lymph nodes (Fig 5P), and the development of FDCs, determined seven days after transfer, was similar between adult and aged mice (Fig 5Q), suggesting that the lymphotoxin-beta receptor-dependent capacity of MRCs to differentiate into FDC was not affected by age. Taken together these data suggest that the activation and proliferation of MRCs induced by immunization is uniquely diminished in an aged setting, resulting in fewer FDCs within the GC after immunization.

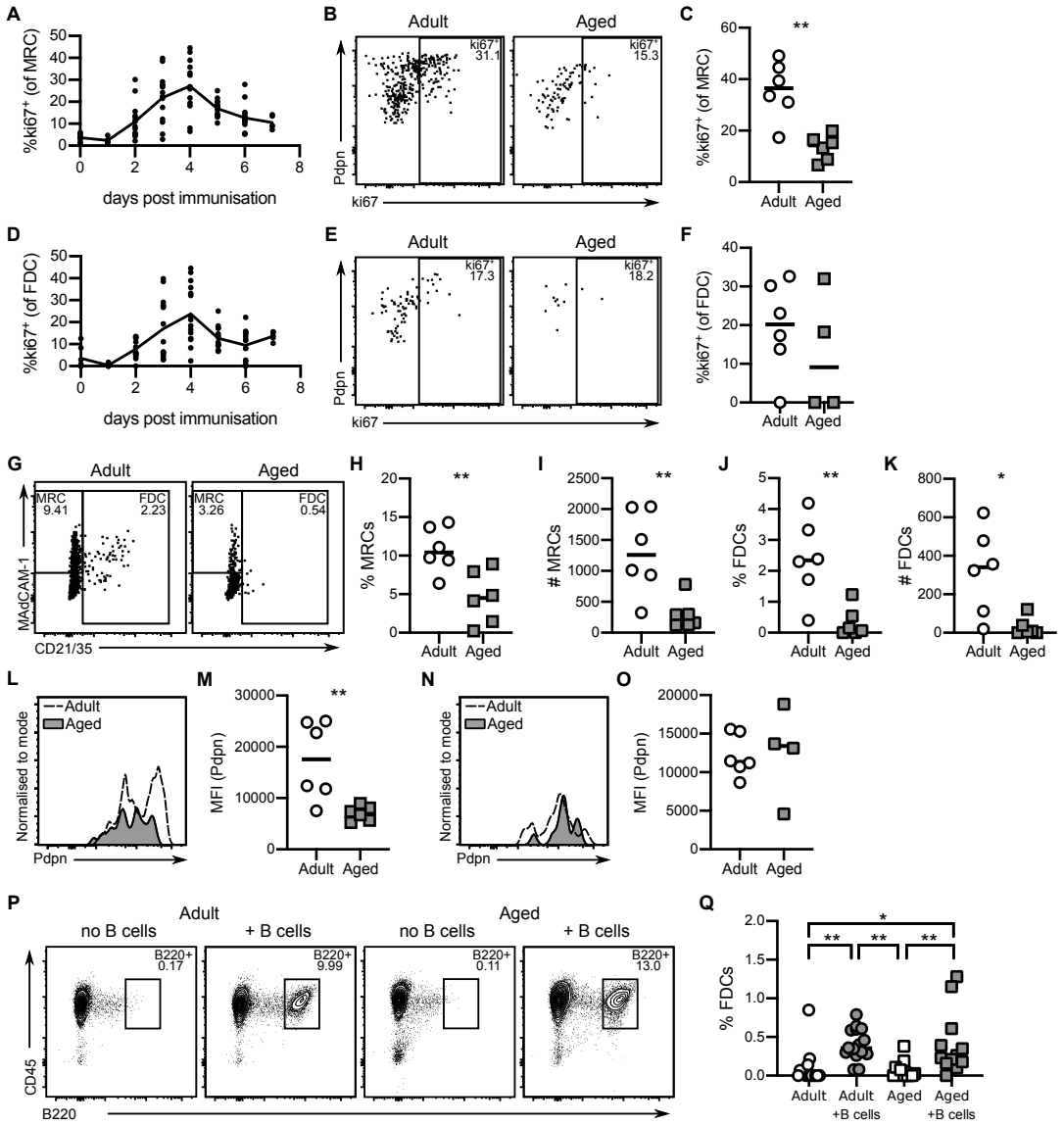

Figure 5. Aged MRCs fail to proliferate in response to immunization. (A) The proliferation of MRCs in response to immunization was determined over a timecourse in adult mice. (B-C) The proliferation of MRCs four days after immunization in adult and aged C57BL/6 mice was determined by ki67 staining (B) and determined as a proportion of MRCs (C). (D) The proliferation of FDCs in response to immunization was determined over a timecourse in adult mice. (E-F) The proliferation of FDCs four days after immunization in adult and aged C57BL/6 mice was determined by ki67 staining (E) and determined as a proportion of FDCs (F). (G-K) The expansion of MRCs and FDCs was determined four days after immunization in adult and aged mice by MAdCAM-1 and CD21/35 staining (G). Both the proportion (H, J) and number (I, K) of MRCs (H, I) and FDCs (J, K) were determined. (L-O) The activation of FDCs (L, M) and MRCs (N, O) was also determined by the mean fluorescence intensity of Pdpn (L, N), as measured by flow cytometry (M, O). (P-Q) Purified C57BL/6 B cells were adoptively transferred into adult (8-12 week old) and aged (>95 week old) B cell-deficient (uMT$^{-/-}$) mice (P). Seven days later the development of FDCs (CD21/35^{+}) was determined as a proportion of Pdpn^{+}CD31^{-}CD45^{-} stromal cells (Q). Data in (B, C, E, F, G-O) are representative of three independent experiments with 5-8 mice per group. Statistical significance was conducted using a Mann-Whitney rank test. Data in (A, D) are combined of three separate experiments comprising 4-6 mice per timepoint. Data in (P, Q) are combined of three independent experiments, comprising 3-5 mice per group. Statistical significance was determined using a one-way ANOVA with Tukey's multiple comparison test. Each symbol represents a biological replicate and lines indicate the mean. * $p<0.05$, ** $p<0.01$ *** $p<0.001$ **** $p<0.0001$.

The poor aged GC response is primarily driven by defects in the aged lymph node microenvironment

The data above demonstrate that MRCs are poorly responsive to vaccination in aged mice, and this is linked to poor expansion of the FDC network and a reduction in GC size. These effects could be due to defects intrinsic to the stroma, or secondary to the poor activation of immune cells, such as T cells. In order to test whether the age of the microenvironment was a key driver of the diminished GC response in aged mice, we established a heterochronic parabiosis model in which the effect of age on the immune cells could be distinguished from the effect of age on the lymph node microenvironment (Fig 6A). Parabiosis is a procedure through which the circulatory system of animals is surgically conjoined, generating a system in which blood-derived cells are shared across individual mice and non-migratory cells, such as stromal cells, remain that of the original host (Conboy et al., 2005). Heterochronic parabiosis has been used to demonstrate that aged lymph nodes are less capable of supporting T cell immigration and survival than lymph nodes from adolescent-adult mice (Davies et al., 2018). Moreover, circulatory factors cannot rejuvenate the cellularity of the aged lymph node (Davies et al., 2018), thus this is an ideal system in which we can determine whether the aged microenvironment impacts on GC formation.

We generated three groups of parabiotic pairs using congenically distinct mice: an adult isochronic group, where adult mice were parabiosed with mice of the same age (6-12 weeks; red); an old isochronic group, where aged mice were parabiosed with aged mice (>92 weeks; blue); and a heterochronic group, where younger adult (6-12 weeks) mice were parabiosed with aged (>92 weeks) mice (purple) (Fig 6A). Because the mice are congenically marked (CD45.1 or CD45.2) we can determine the ability of B cells from adult or aged mice to generate a GC response in both adult and aged lymph nodes. This system also enables evaluation of how stromal cells respond to immunization when exposed to immune cells from mice of different ages. Mice were cohoused in pairs for two weeks prior to surgery to allow for social conditioning and rested for three weeks after surgery to allow revascularization and establishment of parabiosis. Mice were immunized on outer flanks (contralateral to the surgical site) and seven days after immunization we determined stromal cell responses and GC formation (Fig 6B). Mice become T cell lymphopenic with age (Lazuardi et al., 2005), meaning that in adult:aged pairs adult-derived T cells typically predominate in both mice, while aged:aged mice are often mismatched for T cell parabiosis due to variability in T cell lymphopenia (Fig S4). Therefore, the degree of parabiosis was determined by CD45.1:CD45.2 chimerism of B cells in the blood of parabiotic pairs (Fig 6C). We found no significant difference in the establishment of blood parabiosis between the groups, although it is important to note that the aged isochronic group was highly variable.

To understand the contribution of age to the generation of GC B cells, we first determined the size of the total GC response in adult:adult isochronic, aged:aged isochronic and adult:aged heterochonic mice by measuring the proportion of ki67^{+}Bcl-6^{+} GC B cells amongst B220^{+}CD4^{-} B cells (Fig 6D). Consistent with an age-associated defect in GC formation, the aged isochronic pairs had fewer GC B cells than adult isochronic pairs (Fig 6D, E). In heterochronic pairs, the magnitude of the GC reaction was dictated by the age of the host: the GC response was significantly reduced in aged animals, despite the B cell pool deriving from both adult and aged mice (Fig 6E). This demonstrates that the age of the microenvironment dictated the size of the GC response. To determine whether B cell-intrinsic ageing influences their capacity to participate in the GC, we determined the response of adult B cells within aged or adult hosts. B cells from adult mice were impaired in their capacity to generate GC B cells in an aged lymph node (Fig 6F). In agreement with this, B cells from aged mice were as able to participate in the GC response as B cells from younger

adult mice if they were in a younger lymph node (Fig 6F). Taken together, these data suggest that the age of the lymph node microenvironment, rather than that of the B cells, dictates their capacity to generate GC responses in an aged setting.

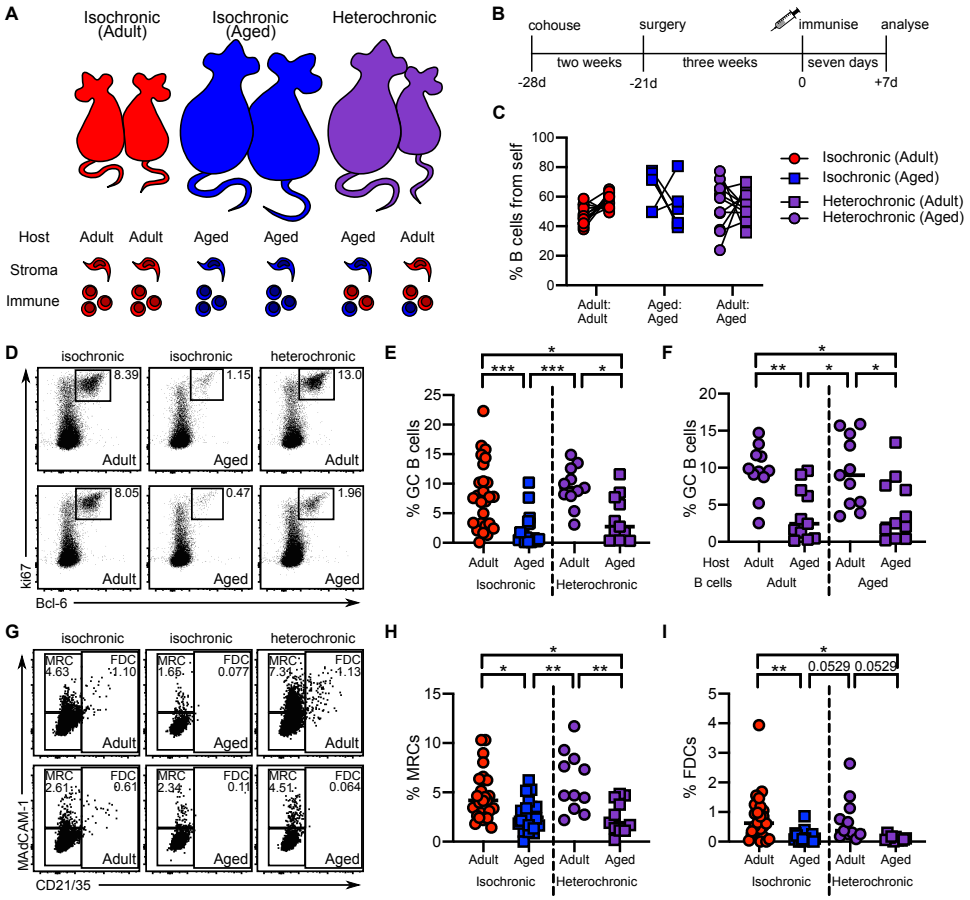

Figure 6. The poor GC and stromal cell response in ageing is driven by the lymph node microenvironment. Heterochronic parabiosis was used to determine the role of the aged lymph node microenvironment in the generation of the GC response. Congenically distinct (CD45.1$^+$ or CD45.2$^+$) C57BL/6 mice were paired in isochronic (adult:adult, red; or aged:aged blue) parabionts or heterochronic (adult:aged purple) parabionts. Adult mice (7-12 week old) are represented with circles; aged mice (>92 week old) are represented with squares. (A) Depicts the experimental groups and the age of relevant cell types in the lymph node in each group. (B) Experimental protocol: mouse pairs were cohoused for two weeks, then surgically joined; three weeks after surgery mice were immunized with 50µg NP-KLH emulsified in Alum subcutaneously on the outer flanks; seven days after immunization the stromal and GC responses were determined by flow cytometry. (C) Successful parabiosis was determined by the blood B cell chimerism; mice with 40-80% self-derived B cells were used for further analyses. (D-F) The GC response was measured by ki67$^+$Bcl-6$^+$ staining (D), and determined as a proportion of B220$^+$ B cells (E). Within heterochronic parabionts, B cells were gated based on age using congenic markers, and their capacity to generate a GC response within adult or aged hosts was determined (F). (G-I) The stromal cell response was measured using MAdCAM-1 and CD21/35 staining (G); the proportion of MRCs (MAdCAM-1$^+$CD21/35$^-$) (H) and FDCs (CD21/35$^+$MAdCAM$^{+/-}$) (I) were determined as a proportion of CD31$^-$CD45$^-$ Pdpn$^+$ stromal cells. Data are combined from six separate experiments, using 4-20 mice per group (2-10 pairs). Data in (C) show individual mice with lines connecting paired blood samples. In (E, F, H, I) each data point represents an individual mouse; individual mice from isochronic parabionts are represented as a single group. Responses to immunization are independent; blood samples are paired. Statistical significance was determined using a two-way ANOVA with Sidak's multiple comparison test (c) or a one-way ANOVA with Holm-Sidak's multiple comparison test (e, f, h, i). * p<0.05, **p<0.01 ***p<0.001 ****p<0.0001.

To determine whether the stromal cell response to immunization was similarly driven by the age of the microenvironment, and not altered by the presence of lymphocytes from an animal of a different age, we measured the expansion of MRCs and FDCs as a proportion of CD45$^-$CD31$^-$Pdpn$^+$ stromal cells (Fig 6G). As observed for the GC responses, the expansion of

MRCs (Fig 6H) and FDCs (Fig 6I) was significantly diminished in the aged isochronic mice, compared to the adult isochronic mice, in line with our previous findings in aged mice (Fig 1). In heterochronic parabionts, we observed that the expansion of MRCs was significantly diminished the aged mouse compared to its adult partner (Fig 6H). A similar trend was observed for the expansion of FDCs in heterochronic parabionts, where FDCs fail to expand in aged mice (Fig 6I). We conclude that age-associated defects in stromal cells, or their microenvironment, and not lymphoid-intrinsic defects, are the primary driver of the poor response of stromal cells to immunization, and that this is a key contributor to the impaired GC response observed in older individuals.

Discussion

The magnitude of the GC response to immunization is reduced in older individuals, and this is linked to poor humoral immunity in a number of settings (Ciabattini et al., 2018; Goodwin et al., 2006; Govaert et al., 1994). In this study we show that stromal cell responses to immunization are impaired in aged mice, and using *in silico* modelling we show that the diminished number of FDCs directly contributes to reduced GC size and output, independent of antigen capture. This indicates that the impaired FDC response to immunization in aged animals contributes to the reduced size of the GC. To understand how immunization directly impacts on stromal cells, we performed RNA sequencing on stromal cells isolated very early after immunization. Surprisingly, FDCs had a small response to immunization, but the transcriptome of their precursors, MRCs (Jarjour et al., 2014), was changed to a large extent after immunization. Age did not have a significant impact on the FDC transcriptome, either before or after immunization. Rather, we found that while age had a small impact on the MRC transcriptome in unimmunized mice, it significantly impaired the responsiveness of MRCs to immunization, leading to impaired proliferation. We also found that the age-associated changes to the microenvironment, of which the stroma are a key part, dictates the size of the GC response irrespective of the age of immune cells. Taken together, our data indicate that ageing causes cell-intrinsic defects in the lymph node stroma. This limits their responsiveness to immunization, impairing expansion and differentiation of the stromal cell network that is necessary to support optimal GC responses.

Diminution of the paracortical stromal cell network has been observed in aged mice (Becklund et al., 2016; Masters et al., 2018; Turner and Mabbott, 2017b) and this has been linked to the reduction in T cell responses observed in aged mice (Lefebvre et al., 2016; Lefebvre et al., 2012; Richner et al., 2015). Ageing also leads to a decrease in the size and number of FDCs (Szakal et al., 2002; Szakal et al., 1990; Turner and Mabbott, 2017b), impaired FDC maturation in response to immunization (Aydar et al., 2002, 2003), and a reduction in antigen capture (Aydar et al., 2003; Turner and Mabbott, 2017b) correlating with poor FDC responses and impairment of the GC in ageing. Our data corroborate these findings, and extend this work to identify poor MRC differentiation as the likely mechanism behind the impaired stromal cell response.

MRCs are a poorly defined lymph node stromal cell subset. They reside beneath the subcapsular sinus (SCS), overlaying the B cell follicle and the interfollicular regions and form a reticular layer that retains lymphoid tissue organizer-like properties (Katakai, 2012; Katakai et al., 2008) that allow them to act as progenitors (Jarjour et al., 2014). MRCs play a role in regulating the SCS macrophage niche (Camara et al., 2019) and are thought to support the localization and survival of innate lymphoid cells in the interfollicular niche through provision of interleukin-7 (Hoorweg et al., 2015). The interfollicular region is also an important site for the initiation of humoral immunity (Gaya et al., 2015) in part through the recruitment of NKT cells that promote humoral immunity (Gaya et al., 2018), and our

transcriptomic data suggest that MRC activation may play a role in directing this, for example through upregulation of *Ccl20* and *Il33* expression. MRC-like stromal cells in the interfollicular region are also key to anti-helminth responses, promoting *de novo* B cell follicle formation (Dubey et al., 2019) and potentially contributing to T cell-mediated type 2 immunity (Leon et al., 2012). Intriguingly these MRC-like cells did not differentiate into FDCs in the newly developed follicles, suggesting that FDC differentiation is not always the ultimate fate of stimulated MRCs. How MRCs integrate immune and pathogen-driven signals is not known, and it is tempting to speculate that lymph node stromal cells act as a rheostat for the induction of pathogen-appropriate adaptive immunity.

Our knowledge of lymph node stromal cells is in its infancy. Our study shows that MRCs play a key role in the formation of GCs in response to immunization, and that their impaired responsiveness in ageing is an important barrier to effective immunity in older individuals. Targeting stromal cells offers a novel avenue through which vaccine efficacy could be improved in older individuals, although further work is required to understand the nuances in stromal cell responses to different immune challenges.

Material and Methods

Mice

C57BL/6, Balb/c, uMT$^{-/-}$ and *Fap*^{tTA}::*TetO*^{cre}::*Rosa26*$^{lox\text{-}stop\text{-}lox\text{-}tdTomato}$ (Denton et al., 2019) mice were bred and housed in the Babraham Institute Biological Support Unit. No primary pathogens or additional agents listed in the FELASA recommendations were detected during health monitoring surveys of the stock holding rooms. Ambient temperature was 19-21°C and relative humidity 52%. Lighting was provided on a 12-hour light: 12-hour dark cycle including 15 min 'dawn' and 'dusk' periods of subdued lighting. After weaning, mice were transferred to individually ventilated cages (GM 500: Techniplast) with 1-5 mice per cage. Mice were fed CRM (P) VP diet (Special Diet Services, #801722) ad libitum and received seeds (e.g., sunflower, millet) at the time of cage-cleaning as part of their environmental enrichment. All UK mouse experimentation was approved by the Babraham Institute Animal Welfare and Ethical Review Body and the UK Home Office. Animal husbandry and experimentation was conducted in accordance with existing European Union and United Kingdom Home Office legislation and local standards. Parabiosis experiments were conducted at the Animal Research Centre, University of Leuven, Belgium using aged C57BL/6 mice purchased from Charles River (UK) or C57BL/6 and CD45.1+ mice bred and aged in-house. All Belgian mice were housed under specific pathogen-free conditions and fed ssniff® R/M-H chow (4.7% w/v sugar, 3.3% w/v fat, 19% w/v protein) and were used in accordance the University of Leuven Animal Ethics Committee and existing European Union standards. Adult mice were 8-12 weeks old and aged mice were 90-105 weeks old when used for experiments. All experiments were conducted use sex-matched controls, and both male and female cohorts were used.

Immunizations

Mice were immunized with 50µg of NP-KLH (4-hydroxy-3-nitrophenylacetyl-Keyhole Limpet Hemocyaninin; conjugation ratio 29-33, Biosearch technologies N-5060) dissolved in PBS at 2mg/mL and emulsified at a 1:1 ratio with Imject Alum Adjuvant (ThermoFisher Scientific 77161). Mice received 50µL subcutaneously on each flank at the inguinal lymph node site under inhalation anesthesia. Lymph nodes were harvested after two, four, seven, 14 or 21 days and processed for analysis. Parabionts were immunized on the upper and lower flanks, draining the axillary and brachial lymph nodes as well as the inguinal site. Lymph nodes in parabiosis experiments were harvested seven days after immunization. Blood samples were

collected by cardiac puncture at the time of dissection to determine blood chimerism for parabiotic pairs.

Parabiosis

Parabiosis was conducted essentially as described (Bunster and Meyer, 1933; Conboy et al., 2005; Wright et al., 2001). Congenically distinct (CD45.1 and CD45.2) female C57BL/6 mice were cohoused for two weeks prior to surgery to ensure harmonious cohabitation. Surgery was conducted under inhalation anesthesia according to LASA Dhiel guidelines. One incision was made from elbow to knee on corresponding lateral sides and the skin separated from the subcutaneous fascia by blunt dissection. The right olecranon of one mouse was attached to the left olecranon of the second mouse with a single suture; this was repeated for the knee joint. The dorsal and ventral skins were anastomosed by continuous suture. Mice we administered analgesia (10mg/kg Carprofen) intraperitoneally twice daily for 48hr. Parabionts were housed as single pairs with free access to food and water and monitored daily for clinical signs. Mice that appeared in distress (hunching, piloerection) were humanely killed. Three weeks after surgery, mice were immunized as above on the outer flanks. Seven days after immunization, blood and lymph node samples were collected and analyzed. Mice that failed to parabiose (<20% of B cells from the partner mouse) were excluded from further analysis.

Cell isolation

For analysis of stromal cells, single cell suspensions were generated by enzymatic digestion as described (Denton et al., 2019; Denton et al., 2014). Briefly, lymph node capsules were pierced with fine forceps and incubated with 0.5mL digestion buffer at 37°C for 20mins and tubes inverted every 5min. After 20mins lymph nodes were triturated with a 1mL pipette tip and supernatant containing released cells was collected to ice-cold buffer comprising PBS containing 2% FCS and 2mM EDTA. Remaining lymph node fragments were digested twice more as described, triturating with a 1mL pipette at 5min intervals. Digestion buffer comprised 0.2mg/mL Collagenase P (Sigma, #11213865001), 0.8 mg/mL Dispase II (Sigma #4942078001) and 0.1mg/mL DNase I (Sigma, #10104159001) in RPMI 1640 media (Gibco, #11875093). Cell suspensions were passed through a 70μm mesh prior to staining. For analysis of GC B cells, lymph nodes were forced through a 40μm mesh in PBS containing 2% FCS. In some experiments GC B cells were analyzed from single cell suspensions prepared by enzymatic digestion, as for stromal cell analysis.

Flow cytometry

Cells were stained using cocktails of antibodies. Fc receptors were blocked prior to staining using anti-CD16/32 (93, ThermoFisher Scientific). Where >1 brilliant violet or brilliant UV dye was used concurrently, cells were stained using BD brilliant stain buffer (BD Biosciences #563794). Cells were fixed and permeabilized for intracellular/nuclear staining using the eBioscience Foxp3/ Transcription Factor Fixation/Permeabilization Staining buffer set (ThermoFisher Scientific, #00-5523-00). Samples were stained for 1hr at 4°C (extracellular) or room temperature (intracellular/nuclear) and fixed/permeabilized for 30mins at 4°C. Antibodies used were: CD45 (30-F11, BioLegend), CD31 (MEC13.3, Biolegend or BD Biosciences), Pdpn (8.8.1, ThermoFisher Scientific), MAdCAM-1 (MECA-367, BioLegend), CD21/35 (7E6, BioLegend; eBio8D9, ThermoFisher Scientific), ICAM (YN1/1.7.4, BioLegend), VCAM (MVCAM.A, BioLegend), CD44 (IM7, BioLegend), ki67 (SolA15, ThermoFisher Scientific), B220 (RA3-6B2, BioLegend), CD4 (GK1.5 or RM4-5, BioLegend or ThermoFisher Scientific), Bcl-6 (K112-91, BD Biosciences). In some experiments biotinylated antibodies were detected with BUV-395-conjugated streptavidin (BD Biosciences, #564176). Dead cells were excluded with Fixable live/dead e780 (ThermoFisher Scientific, #65-0865-18). Samples

were acquired on a BD LSRFortessa (BD Biosciences) harbouring 355, 405, 488, 561 and 640nm lasers and analyzed using FlowJo software (TreeStar).

Immunofluorescence and confocal microscopy

Lymph nodes were immersion-fixed in periodate-lysine-paraformaldehyde containing 1% PFA (Sigma #P6148), 0.075 M L-lysine (Sigma #L5501), 0.37 M sodium phosphate (pH 7.4, Sigma #342483), and 0.01 M NaIO4 (Sigma #210048) for five hours at 4°C, washed, cryoprotected in 30% sucrose (Sigma #S0389) overnight at 4°C, embedded in optimal cutting temperature medium (VWR #25608-930) on a dry ice/ethanol bath and stored at -80°C. Sections (20μm) were cut at -16°C on a cryostat (Leica), air-dried overnight and stored at -20°C (short-term) or -80°C (long-term). For staining, sections were defrosted and air-dried overnight at room temperature, rehydrated with PBS containing 0.05% Tween-20 (PBST), permeabilized with 2% Triton X-100 (Sigma #X100) for 15min at room temperature and blocked in PBST containing 1% BSA for 1hr at room temperature. Tissues sections were stained with antibodies directed against CD35-biotin (8C12, BD Biosciences), ki67-FITC (SolA15, ThermoFisher Scientific), IgD-AF594 (11-26c.2a, BioLegend) and CD3-APC (17A2, ThermoFisher Scientific) overnight at 4°C. Biotinylated CD35 was detected with BV421-conjugated streptavidin (BioLegend, #405225) for 2hr at room temperature. Sections were washed, mounted in aqueous mounting media (HydroMount; National Diagnostics, #HS-106) and allowed to dry prior to imaging. Sections were obtained using a Zeiss LSM880 harboring 405-, 432-, 488-, 561-, and 633-nm lasers using 20×/0.50 air or 40×/1.40 oil objectives. Image channels were collected separately and analyzed and compiled using Fiji (National Institutes of Health) software. FDC and GC areas were calculated using CellProfiler (McQuin et al., 2018): the GC area (μm^2) was defined as $IgD^-ki67^+CD35^+$; analysis was performed using automated identification of GCs, with the light zone FDC network area (μm^2) defined as IgD^-CD35^+.

Mathematical modelling of GC output

In silico mathematical modelling was carried out using the *hyphasma* model, as described in (Meyer-Hermann et al., 2012). Briefly, the GC is modelled as a grid within a sphere; each grid point is the size of a cell (5μm) and has a defined concentration of the DZ and LZ chemokines, CXCL12 and CXCL13, respectively. Each simulated cell's properties, that is position, polarity, velocity, antigen receptor, and amount of internalized antigen, are updated at each time-step and can be monitored computationally. The direction of movement is described by a persistent time and a distribution of turning angles that is influenced by chemotaxis. GC B cells are separated into proliferating centroblasts in the DZ and centrocytes undergo selection in the LZ. The proliferation, death and selection of GC B cells are incorporated as probabilistic events depending on the affinity of the receptor and the interaction with FDCs or Tfh cells. Stellate FDCs are spread randomly in a fraction of the sphere defined as the LZ and the total amount of antigen is spread equally between all grid positions occupied by FDCs. In each simulation, B cells undergo selection based on antigen abundance, antigen uptake and the probability of Tfh cell encounter. Each simulation models the typical GC steps where B cells first search for, and acquire, antigen from FDCs, then search for, and interact with, Tfh cells to receive a proliferation signal before exiting the GC or recycling to the DZ. Tfh cell help is given to interacting B cells with the highest amount of antigen, which also indicates B cell receptor affinity, and the model assumes that centrocytes interact with Tfh cells once per cycle. In the model used here, the GC is seeded with two B cell clones per hour over the first three days, each of which divides six times (Arulraj et al., 2019); this models the *in vivo* findings that 10-100 B cell clones seed a founder GC (Tas et al., 2016). A full list of parameters is available in (Robert et al., 2017).

Adoptive transfer
Spleens from 8-week-old wildtype mice were forced through a 40mm sieve and B cells were enriched using the MagniSort B cell enrichment kit (ThermoFisher Scientific, 8804-6827-74) according to manufacturer's instructions. Mice were administered 2-4 million B cells intravenously via the tail vein.

RNA Sequencing and analysis
Stromal cells were released from lymph nodes by enzymatic digestion as described above. Hematopoietic cells were depleted using anti-CD45 microbeads (Miltenyi Biotec, 130-052-301) (7μL/10^7 cells), a QuadroMACS magnet (Miltenyi Biotec) and LS columns (Miltenyi Biotec, 130-042-401), according to manufacturer's instructions. The $CD45^-$ fraction was retained and stained with live-dead e780 and antibodies directed against CD45, Pdpn, CD31, MAdCAM-1 and CD21/35 as described above. MRCs (MAdCAM-1^+CD21/35^-Pdpn$^+$CD31^-CD45^-) or FDCs (MAdCAM-1^+CD21/35^+Pdpn$^+$CD31^-CD45^-) from unimmunized or immunized adult (8 week old) and aged (>95 week old) mice were sorted directly into 8.5μL of lysis buffer supplied with the SMART-Seq v4 Ultra low Input RNA kit for Sequencing (Clontech #634890). Where possible we matched the number of sorted FDCs (28-342 in unimmunized, 18-82 in immunized) and MRCs (263-798 in unimmunized, 188-520 in immunized) between adult and aged samples at each time point to limit input cell number variation in the sequencing data.

cDNA from sorted cells was generated using the SMART-Seq v4 Ultra low input RNA kit (Clontech # 634890) according to manufacturer's instructions. Libraries were prepared with 400pg of cDNA per sample using the Illumina Nextera XT kit (#FC-131-1096) following manufacturer's instructions. cDNA and sequencing library quality were determined using Agilent BioAnalyser High Sensitivity DNA chips (#5067-4626), Qubit dsDNA High sensitivity Assay kit (Invitrogen #Q32854) on a Qubit 4 fluorometer (Invitrogen), and a KAPA library quantification kit (Roche #7960140001). Samples were sequenced on a HiSeq 2500 (Illumina, v4 chemistry) as 100bp single-end reads. Analysis was performed using the SeqMonk software package (Babraham Institute, https://www.bioinformatics.babraham.ac.uk/projects/seqmonk/, version 1.45.4) after trimming (Trim Galore v0.4.2) and alignment of reads to the reference mouse genome GRCm38 using HISAT2 (Kim et al., 2015). Reads were quantitated over exons and library size was standardized to reads per million, and then read counts were log2 transformed. Data were analyzed by cell type. Expressed genes were defined as those with a log2(reads per million)>-4 in at least five biological replicates. Principal component analysis was conducted using all expressed genes. Differentially expressed genes ($p<0.05$, $\log_2 fc>1$) were identified using Seqmonk's built-in DESeq2 analysis (Love et al., 2014) of raw counts in pairwise comparisons: cells from unimmunized adult mice were compared to cells from unimmunized aged mice; and immunized cells were compared to unimmunized cells for both aged and adult mice. Differentially expressed genes ($p<0.05$) with a $\log_2 fc>1$ in adult, but not aged, samples were used for gene ontology analysis, which was conducted using Gorilla (http://cbl-gorilla.cs.technion.ac.il/) against a list of background genes; gene ontology terms were refined using Revigo (http://revigo.irb.hr/), with a small gene list (allowed similarity = 0.5) output.

Statistics
Experiments were repeated a minimum of two times; in some analyses independent experiments were combined. Data were analyzed and visualized using Prism 8 (GraphPad). Statistical significance was determined using the Mann-Whitney rank test where two groups were compared, or a one- ANOVA with Tukey's or Holm-Sidak's multiple testing correction or two-way ANOVA with Sidak's multiple testing correction where >2 groups were

compared. P-values <0.05 were considered statistically significant. In graphs, each data point represents a biological replicate and lines indicate the mean.

Acknowledgements
We thank staff from the Biological Support Unit and Flow Cytometry and Imaging Facilities (Babraham Research Campus) for support.

AED was supported by a Biotechnology and Biological Sciences Research Council Future Leader Fellowship (BB/N011740/1), ASC was supported by European Union's Horizon 2020 research and innovation programme "ENLIGHT-TEN" under the Marie Sklodowska-Curie grant agreement No.: 675395, DLH was supported by a National Health and Medical Research Council Australia Early-Career Fellowship (APP1139911). This work was supported by an H2020 European Research Council grant to MAL (637801 TWILIGHT), a Biotechnology and Biological Sciences Research Council grants to MAL (BBS/E/B/000C0408 and BBS/E/B/000C0407), an European Research Council Consolidator grant to AL (TissueTreg), a Human Frontier Science Program grant to MMH (RGP0033/2015), and a Biotechnology and Biological Sciences Research Council Campus Capability grant to the Babraham Institute.

Author Contributions
AED designed the study, conducted experiments, analyzed results, acquired funding and wrote the manuscript. ASC conducted experiments and analyzed results. JD, DLH and PR conducted experiments and provided scientific advice. EJC supervised data analysis and provided scientific advice. MMH and AL supervised research and edited the manuscript; MAL designed the study, supervised research, acquired funding and wrote the manuscript. All authors read, edited and approved the manuscript.

Declaration of Interests
The authors declare no competing interests.

Lead contact
Further information and requests for resources and reagents should be directed to and will be fulfilled by the Lead Contact, Alice Denton (a.denton@imperial.ac.uk)

References
Alexandre, Y.O., and Mueller, S.N. (2018). Stromal cell networks coordinate immune response generation and maintenance. Immunol Rev *283*, 77-85.
Allen, C.D., Ansel, K.M., Low, C., Lesley, R., Tamamura, H., Fujii, N., and Cyster, J.G. (2004). Germinal center dark and light zone organization is mediated by CXCR4 and CXCR5. Nat Immunol *5*, 943-952.
Allen, C.D., and Cyster, J.G. (2008). Follicular dendritic cell networks of primary follicles and germinal centers: phenotype and function. Semin Immunol *20*, 14-25.
Arulraj, T., Binder, S.C., Robert, P.A., and Meyer-Hermann, M. (2019). Synchronous Germinal Center Onset Impacts the Efficiency of Antibody Responses. Front Immunol *10*, 2116.
Aydar, Y., Balogh, P., Tew, J.G., and Szakal, A.K. (2002). Age-related depression of FDC accessory functions and CD21 ligand-mediated repair of co-stimulation. Eur J Immunol *32*, 2817-2826.
Aydar, Y., Balogh, P., Tew, J.G., and Szakal, A.K. (2003). Altered regulation of Fc gamma RII on aged follicular dendritic cells correlates with immunoreceptor tyrosine-based inhibition motif signaling in B cells and reduced germinal center formation. J Immunol *171*, 5975-5987.

Bajenoff, M., Egen, J.G., Koo, L.Y., Laugier, J.P., Brau, F., Glaichenhaus, N., and Germain, R.N. (2006). Stromal cell networks regulate lymphocyte entry, migration, and territoriality in lymph nodes. Immunity *25*, 989-1001.
Bannard, O., Horton, R.M., Allen, C.D., An, J., Nagasawa, T., and Cyster, J.G. (2013). Germinal center centroblasts transition to a centrocyte phenotype according to a timed program and depend on the dark zone for effective selection. Immunity *39*, 912-924.
Becklund, B.R., Purton, J.F., Ramsey, C., Favre, S., Vogt, T.K., Martin, C.E., Spasova, D.S., Sarkisyan, G., LeRoy, E., Tan, J.T.*, et al.* (2016). The aged lymphoid tissue environment fails to support naive T cell homeostasis. Sci Rep *6*, 30842.
Boraschi, D., Aguado, M.T., Dutel, C., Goronzy, J., Louis, J., Grubeck-Loebenstein, B., Rappuoli, R., and Del Giudice, G. (2013). The gracefully aging immune system. Sci Transl Med *5*, 185ps188.
Bunster, E., and Meyer, R.K. (1933). An improved method of parabiosis. The Anatomical Record *57*, 339-343.
Camara, A., Cordeiro, O.G., Alloush, F., Sponsel, J., Chypre, M., Onder, L., Asano, K., Tanaka, M., Yagita, H., Ludewig, B.*, et al.* (2019). Lymph Node Mesenchymal and Endothelial Stromal Cells Cooperate via the RANK-RANKL Cytokine Axis to Shape the Sinusoidal Macrophage Niche. Immunity *50*, 1467-1481 e1466.
Ciabattini, A., Nardini, C., Santoro, F., Garagnani, P., Franceschi, C., and Medaglini, D. (2018). Vaccination in the elderly: The challenge of immune changes with aging. Semin Immunol *40*, 83-94.
Conboy, I.M., Conboy, M.J., Wagers, A.J., Girma, E.R., Weissman, I.L., and Rando, T.A. (2005). Rejuvenation of aged progenitor cells by exposure to a young systemic environment. Nature *433*, 760-764.
Cremasco, V., Woodruff, M.C., Onder, L., Cupovic, J., Nieves-Bonilla, J.M., Schildberg, F.A., Chang, J., Cremasco, F., Harvey, C.J., Wucherpfennig, K.*, et al.* (2014). B cell homeostasis and follicle confines are governed by fibroblastic reticular cells. Nat Immunol *15*, 973-981.
Davies, J.S., Thompson, H.L., Pulko, V., Padilla Torres, J., and Nikolich-Zugich, J. (2018). Role of Cell-Intrinsic and Environmental Age-Related Changes in Altered Maintenance of Murine T Cells in Lymphoid Organs. J Gerontol A Biol Sci Med Sci *73*, 1018-1026.
Denton, A.E., Carr, E.J., Magiera, L.P., Watts, A.J.B., and Fearon, D.T. (2019). Embryonic FAP(+) lymphoid tissue organizer cells generate the reticular network of adult lymph nodes. J Exp Med *216*, 2242-2252.
Denton, A.E., and Linterman, M.A. (2017). Stromal networking: cellular connections in the germinal centre. Curr Opin Immunol *45*, 103-111.
Denton, A.E., Roberts, E.W., Linterman, M.A., and Fearon, D.T. (2014). Fibroblastic reticular cells of the lymph node are required for retention of resting but not activated CD8+ T cells. Proc Natl Acad Sci U S A *111*, 12139-12144.
Dubey, L.K., Ludewig, B., Luther, S.A., and Harris, N.L. (2019). IL-4Ralpha-Expressing B Cells Are Required for CXCL13 Production by Fibroblastic Reticular Cells. Cell Rep *27*, 2442-2458 e2445.
Eaton, S.M., Burns, E.M., Kusser, K., Randall, T.D., and Haynes, L. (2004). Age-related defects in CD4 T cell cognate helper function lead to reductions in humoral responses. J Exp Med *200*, 1613-1622.
Fu, Y.X., Huang, G., Wang, Y., and Chaplin, D.D. (1998). B lymphocytes induce the formation of follicular dendritic cell clusters in a lymphotoxin alpha-dependent fashion. J Exp Med *187*, 1009-1018.
Garcia, G.G., and Miller, R.A. (2001). Single-cell analyses reveal two defects in peptide-specific activation of naive T cells from aged mice. J Immunol *166*, 3151-3157.

Gaya, M., Barral, P., Burbage, M., Aggarwal, S., Montaner, B., Warren Navia, A., Aid, M., Tsui, C., Maldonado, P., Nair, U*., et al.* (2018). Initiation of Antiviral B Cell Immunity Relies on Innate Signals from Spatially Positioned NKT Cells. Cell *172*, 517-533 e520.
Gaya, M., Castello, A., Montaner, B., Rogers, N., Reis e Sousa, C., Bruckbauer, A., and Batista, F.D. (2015). Host response. Inflammation-induced disruption of SCS macrophages impairs B cell responses to secondary infection. Science *347*, 667-672.
Goodwin, K., Viboud, C., and Simonsen, L. (2006). Antibody response to influenza vaccination in the elderly: a quantitative review. Vaccine *24*, 1159-1169.
Goronzy, J.J., and Weyand, C.M. (2013). Understanding immunosenescence to improve responses to vaccines. Nat Immunol *14*, 428-436.
Govaert, T.M., Thijs, C.T., Masurel, N., Sprenger, M.J., Dinant, G.J., and Knottnerus, J.A. (1994). The efficacy of influenza vaccination in elderly individuals. A randomized double-blind placebo-controlled trial. JAMA *272*, 1661-1665.
Hoorweg, K., Narang, P., Li, Z., Thuery, A., Papazian, N., Withers, D.R., Coles, M.C., and Cupedo, T. (2015). A Stromal Cell Niche for Human and Mouse Type 3 Innate Lymphoid Cells. J Immunol *195*, 4257-4263.
Jarjour, M., Jorquera, A., Mondor, I., Wienert, S., Narang, P., Coles, M.C., Klauschen, F., and Bajenoff, M. (2014). Fate mapping reveals origin and dynamics of lymph node follicular dendritic cells. J Exp Med *211*, 1109-1122.
Katakai, T. (2012). Marginal reticular cells: a stromal subset directly descended from the lymphoid tissue organizer. Front Immunol *3*, 200.
Katakai, T., Suto, H., Sugai, M., Gonda, H., Togawa, A., Suematsu, S., Ebisuno, Y., Katagiri, K., Kinashi, T., and Shimizu, A. (2008). Organizer-like reticular stromal cell layer common to adult secondary lymphoid organs. J Immunol *181*, 6189-6200.
Kim, D., Langmead, B., and Salzberg, S.L. (2015). HISAT: a fast spliced aligner with low memory requirements. Nat Methods *12*, 357-360.
Kosco, M.H., Burton, G.F., Kapasi, Z.F., Szakal, A.K., and Tew, J.G. (1989). Antibody-forming cell induction during an early phase of germinal centre development and its delay with ageing. Immunology *68*, 312-318.
Krishnamurty, A.T., and Turley, S.J. (2020). Lymph node stromal cells: cartographers of the immune system. Nat Immunol *21*, 369-380.
Lazuardi, L., Jenewein, B., Wolf, A.M., Pfister, G., Tzankov, A., and Grubeck-Loebenstein, B. (2005). Age-related loss of naive T cells and dysregulation of T-cell/B-cell interactions in human lymph nodes. Immunology *114*, 37-43.
Lefebvre, J.S., Masters, A.R., Hopkins, J.W., and Haynes, L. (2016). Age-related impairment of humoral response to influenza is associated with changes in antigen specific T follicular helper cell responses. Sci Rep *6*, 25051.
Lefebvre, J.S., Maue, A.C., Eaton, S.M., Lanthier, P.A., Tighe, M., and Haynes, L. (2012). The aged microenvironment contributes to the age-related functional defects of CD4 T cells in mice. Aging Cell *11*, 732-740.
Leon, B., Ballesteros-Tato, A., Browning, J.L., Dunn, R., Randall, T.D., and Lund, F.E. (2012). Regulation of T(H)2 development by CXCR5+ dendritic cells and lymphotoxin-expressing B cells. Nat Immunol *13*, 681-690.
Link, A., Vogt, T.K., Favre, S., Britschgi, M.R., Acha-Orbea, H., Hinz, B., Cyster, J.G., and Luther, S.A. (2007). Fibroblastic reticular cells in lymph nodes regulate the homeostasis of naive T cells. Nat Immunol *8*, 1255-1265.
Love, M.I., Huber, W., and Anders, S. (2014). Moderated estimation of fold change and dispersion for RNA-seq data with DESeq2. Genome Biol *15*, 550.
Martinez, V.G., Pankova, V., Krasny, L., Singh, T., Makris, S., White, I.J., Benjamin, A.C., Dertschnig, S., Horsnell, H.L., Kriston-Vizi, J*., et al.* (2019). Fibroblastic Reticular Cells Control Conduit Matrix Deposition during Lymph Node Expansion. Cell Rep *29*, 2810-2822 e2815.

Masters, A.R., Jellison, E.R., Puddington, L., Khanna, K.M., and Haynes, L. (2018). Attrition of T Cell Zone Fibroblastic Reticular Cell Number and Function in Aged Spleens. Immunohorizons *2*, 155-163.
McQuin, C., Goodman, A., Chernyshev, V., Kamentsky, L., Cimini, B.A., Karhohs, K.W., Doan, M., Ding, L., Rafelski, S.M., Thirstrup, D*., et al.* (2018). CellProfiler 3.0: Next-generation image processing for biology. PLoS Biol *16*, e2005970.
Meyer-Hermann, M., Mohr, E., Pelletier, N., Zhang, Y., Victora, G.D., and Toellner, K.M. (2012). A theory of germinal center B cell selection, division, and exit. Cell Rep *2*, 162-174.
Meyer-Hermann, M.E., and Maini, P.K. (2005). Cutting edge: back to "one-way" germinal centers. J Immunol *174*, 2489-2493.
Montecino-Rodriguez, E., Berent-Maoz, B., and Dorshkind, K. (2013). Causes, consequences, and reversal of immune system aging. J Clin Invest *123*, 958-965.
Richner, J.M., Gmyrek, G.B., Govero, J., Tu, Y., van der Windt, G.J., Metcalf, T.U., Haddad, E.K., Textor, J., Miller, M.J., and Diamond, M.S. (2015). Age-Dependent Cell Trafficking Defects in Draining Lymph Nodes Impair Adaptive Immunity and Control of West Nile Virus Infection. PLoS Pathog *11*, e1005027.
Robert, P.A., Rastogi, A., Binder, S.C., and Meyer-Hermann, M. (2017). How to Simulate a Germinal Center. Methods Mol Biol *1623*, 303-334.
Rodda, L.B., Bannard, O., Ludewig, B., Nagasawa, T., and Cyster, J.G. (2015). Phenotypic and Morphological Properties of Germinal Center Dark Zone Cxcl12-Expressing Reticular Cells. J Immunol *195*, 4781-4791.
Rodda, L.B., Lu, E., Bennett, M.L., Sokol, C.L., Wang, X., Luther, S.A., Barres, B.A., Luster, A.D., Ye, C.J., and Cyster, J.G. (2018). Single-Cell RNA Sequencing of Lymph Node Stromal Cells Reveals Niche-Associated Heterogeneity. Immunity *48*, 1014-1028 e1016.
Sage, P.T., Tan, C.L., Freeman, G.J., Haigis, M., and Sharpe, A.H. (2015). Defective TFH Cell Function and Increased TFR Cells Contribute to Defective Antibody Production in Aging. Cell Rep *12*, 163-171.
Stebegg, M., Bignon, A., Hill, D.L., Silva-Cayetano, A., Krueger, C., Vanderleyden, I., Innocentin, S., Boon, L., Wang, J., Zand, M.S*., et al.* (2020). Rejuvenating conventional dendritic cells and T follicular helper cell formation after vaccination. Elife *9*.
Stebegg, M., Kumar, S.D., Silva-Cayetano, A., Fonseca, V.R., Linterman, M.A., and Graca, L. (2018). Regulation of the Germinal Center Response. Front Immunol *9*, 2469.
Szakal, A.K., Aydar, Y., Balogh, P., and Tew, J.G. (2002). Molecular interactions of FDCs with B cells in aging. Semin Immunol *14*, 267-274.
Szakal, A.K., Taylor, J.K., Smith, J.P., Kosco, M.H., Burton, G.F., and Tew, J.J. (1990). Kinetics of germinal center development in lymph nodes of young and aging immune mice. Anat Rec *227*, 475-485.
Tas, J.M., Mesin, L., Pasqual, G., Targ, S., Jacobsen, J.T., Mano, Y.M., Chen, C.S., Weill, J.C., Reynaud, C.A., Browne, E.P*., et al.* (2016). Visualizing antibody affinity maturation in germinal centers. Science *351*, 1048-1054.
Turner, V.M., and Mabbott, N.A. (2017a). Influence of ageing on the microarchitecture of the spleen and lymph nodes. Biogerontology *18*, 723-738.
Turner, V.M., and Mabbott, N.A. (2017b). Structural and functional changes to lymph nodes in ageing mice. Immunology *151*, 239-247.
Vinuesa, C.G., Linterman, M.A., Yu, D., and MacLennan, I.C. (2016). Follicular Helper T Cells. Annu Rev Immunol *34*, 335-368.
Wang, X., Cho, B., Suzuki, K., Xu, Y., Green, J.A., An, J., and Cyster, J.G. (2011). Follicular dendritic cells help establish follicle identity and promote B cell retention in germinal centers. J Exp Med *208*, 2497-2510.
Weinberger, B., and Grubeck-Loebenstein, B. (2012). Vaccines for the elderly. Clin Microbiol Infect *18 Suppl 5*, 100-108.

Weisel, F.J., Zuccarino-Catania, G.V., Chikina, M., and Shlomchik, M.J. (2016). A Temporal Switch in the Germinal Center Determines Differential Output of Memory B and Plasma Cells. Immunity *44*, 116-130.
Wright, D.E., Wagers, A.J., Gulati, A.P., Johnson, F.L., and Weissman, I.L. (2001). Physiological migration of hematopoietic stem and progenitor cells. Science *294*, 1933-1936.
Yang, C.Y., Vogt, T.K., Favre, S., Scarpellino, L., Huang, H.Y., Tacchini-Cottier, F., and Luther, S.A. (2014). Trapping of naive lymphocytes triggers rapid growth and remodeling of the fibroblast network in reactive murine lymph nodes. Proc Natl Acad Sci U S A *111*, E109-118.
Yang, X., Stedra, J., and Cerny, J. (1996). Relative contribution of T and B cells to hypermutation and selection of the antibody repertoire in germinal centers of aged mice. J Exp Med *183*, 959-970.